

Correlation mechanism between force chains and friction mechanism during powder compaction

Ning Zhang(张宁) , Shuai Zhang(张帅), Jian-Jun Tan(谈健君), and Wei Zhang(张炜)

Citation: Chin. Phys. B, 2022, 31 (**2**): 024501. DOI: 10.1088/1674-1056/ac0db1
Journal homepage: http://cpb.iphy.ac.cn; http://iopscience.iop.org/cpb

What follows is a list of articles you may be interested in

Influence of particle packing structure on sound velocity

Chuang Zhao(赵闯), Cheng-Bo Li(李成波), Lin Bao(鲍琳)
Chin. Phys. B, 2018, 27 (**10**): 104501. DOI: 10.1088/1674-1056/27/10/104501

Required width of exit to avoid the faster-is-slower effect in highly competitive evacuation

Yu-Chun Zhang(张玉春), Jian Ma(马剑), You-Liang Si(司有亮), Tong Ran(冉桐), Fan-Yu Wu(吴凡雨), Guo-Yuan Wang(王国元), Peng Lin(林鹏)
Chin. Phys. B, 2017, 26 (**8**): 084504. DOI: 10.1088/1674-1056/26/8/084504

Stabilizing effect of plasma discharge on bubbling fluidized granular bed

Hu Mao-Bin, Dang Sai-Chao, Ma Qiang, Xia Wei-Dong
Chin. Phys. B, 2015, 24 (**7**): 074502. DOI: 10.1088/1674-1056/24/7/074502

Experimental study and analysis on the rising motion of grains in a vertically-vibrated pipe

Liu Yu, Zhao Jun-Hong
Chin. Phys. B, 2015, 24 (**3**): 034502. DOI: 10.1088/1674-1056/24/3/034502

Properties of surface waves in granular media under gravity

Zheng He-Peng
Chin. Phys. B, 2014, 23 (**5**): 054503. DOI: 10.1088/1674-1056/23/5/054503

Correlation mechanism between force chains and friction mechanism during powder compaction

Ning Zhang(张宁)†, Shuai Zhang(张帅), Jian-Jun Tan(谈健君), and Wei Zhang(张炜)

School of Mechanical & Automotive Engineering, Fujian University of Technology, Fuzhou 350118, *China*

(Received 10 May 2021; revised manuscript received 19 June 2021; accepted manuscript online 23 June 2021)

The relation between friction mechanism and force chains characteristics has not yet been fully studied in the powder metallurgy research area. In this work, a uniaxial compression discrete element model is established based on the compaction process of ferrous powder. Furthermore, the correlation mechanism between force chains and the friction mechanism during powder compaction is investigated. The simulation results reveal a strong correlation between the variation of the friction coefficient and the evolution of force chains. During the powder compaction, the friction coefficient would eventually tend to be stable, a feature which is also closely related to the slip ratio between particles. The side wall friction and the friction between particles would have an important effect on the direction of force chain growth in about one-third of the area near the side wall. The research results provide theoretical guidance for improving the densification process of the powder according to the force chain and friction.

Keywords: powder compaction, force chains, granular matter, discrete element method

PACS: 45.70.–n, 45.70.Cc, 62.20.Qp, 62.20.–x **DOI:** 10.1088/1674-1056/ac0db1

1. Introduction

Powder metallurgy is a modern manufacturing technology. Green compact can be formed in various ways. These include injection molding,[1] hot isostatic pressing,[2] electromagnetic compaction,[3] die compaction,[4] and others. Uniaxial compression is a most widely used green compact forming technology. During powder compaction, the asymmetrical distribution of green density is caused mainly by friction between particles and the die wall.[5] The friction is the critical factor that creates the uneven particle flow and stress distribution.[6] Therefore, the friction mechanism plays an important role in densifying powders.

Numerous investigations have been conducted on powder compaction and friction behaviour. Shoaib *et al.*[7] investigated the experiment on the uniaxial compression of powder by using a buffer, and improved the green density and the mechanical properties of the green compact. Wang *et al.*[8] found that the elastic spring-back and demolding force during high velocity compaction are smaller than those during traditional compaction. The above studies contributed to the enhancement of green density and the mechanical properties of the green compacts. In recent years, more and more scholars have considered the influence of friction on the green density during powder compaction. Güner *et al.*[9,10] simulated and experimentally investigated the friction behaviour of powder compaction by using the multi-particle finite element method (MPFEM). The influence factors of particle friction coefficient and contact stress were analyzed, and the influence of the friction model on friction coefficient was studied. However, the MPFEM contains few particles, and it might be better to examine the friction with more particles. Chen *et al.*[11] experimentally studied the compaction of dry and wet mixing ferrous-based particles. Testing of the frictional characteristic during compaction revealed that the wet mixing process can realize lubricant uniformity and improve the process of desifying powders. Previous studies regarded powders as a macroscopic continuum medium or as a complex consisting of few deformable particles during powder compaction. Obviously, the investigation on the micro friction mechanism between discrete granules in powder compaction needs to be further studied.

To study discrete particles, Cundall and Strack proposed the discrete element method (DEM).[12] Many scholars have studied granular matter systems by using the said scheme. To date, the discrete element method has been able to carry out not only the microscopic research, but also the macroscopic analysis on granule matter.[13] Furthermore, the concept of the force chain was proposed, and multi-scale mechanical coupling analysis was subsequently made.[14–17] The force chain is a quasi-linear transfer route of force in a particle system that carries larger forces than other particles, along its normal direction.[18] The nonlinear sensitive response of granular material can be obtained by using the force chain which is on a mesoscopic scale in multi-scale mechanics.[13] Therefore, it is necessary to study the evolution of force chain in powder compaction process.

The evolution of the force chain has been studied by numerous researchers. Bouchaud *et al.*[17] proposed a phenomenological equation to describe the propagation of force in granular matter. A variety of force chain retrieval and recogni-

†Corresponding author. E-mail: zhangning138@126.com

© 2022 Chinese Physical Society and IOP Publishing Ltd

tion algorithms appeared, such as the principal stress criterion method[16,18] and the contact force criterion method.[13–15] In addition, some scholars have conducted experimental research on the evolution of force chains. Fang *et al.*[19] studied the arching effect of the force chain through a photo elastic experiment. However, the photo elastic method is unsuitable for an opaque powder, such as ferrous powder. Mahabadi and Jang[20] studied the force chain by x-ray. However, CT-scan is better adapted to the static analysis of powder. Regarding the dynamic change of opaque granular materials, the DEM is a feasible technique for investigating the force chain. Zhang *et al.*[13] employed the contact force criterion method to examine the evolution of the force chains during high velocity compaction (HVC). For geotechnical mechanics, the principal stress criterion method is employed more commonly. The said method mainly analyzes particles with larger or smaller principal stress which must have certain angles and other conditions.[16,21–24] Fu *et al.*[22] studied the force chain evolution of cohesionless granular materials under a biaxial compression and conducted some quantitative researches. Liu *et al.*[25] simulated and evaluated the biaxial compression experiment on cohesive-friction material. The mesoscale force chain was defined and analyzed from the aspects of force chain buckling and local expansion. The principal stress criterion method has less applications in powder compaction. Thus, the said technique should be thoroughly investigated in relation to powder compaction.

To analyze the relation between friction characteristics and force chain, Wang *et al.*[26] used the FEM-DEM coupling method to analyze a three-body friction behavior, and summarized the corresponding relation between the stress distribution in the FEM region and the force chain distribution in the DEM region. Meng and Liu[27] utilized the DEM to study the influence of particle friction on macroscopic mechanical behavior, microscopic mechanical response and the relationship between different particle friction conditions and force chain distribution. The above researches focused mainly on the distribution of the force chain under different friction conditions. Zheng *et al.*[28] experimentally investigated the frictional effects of three different materials, for which the influence of friction on the direction of the force chain was evaluated through photo elastic experiments. This work primarily involved the influence of friction on the direction of the force chain. However, obtaining more data for quantitative analysis through the photo elastic experiment is problematic. Zhang *et al.*[29] employed a contact force criterion to examine the relationship between the friction of the side wall and the networks of contact forces from the macroscopic and microscopic aspects. The friction characteristics between particles need to be studied further.

As mentioned above, some frictional behaviors of particles have been well studied through experiments or DEM numerical simulation. However, the reason for the lower densification degree caused by particle friction is unclear. Thus, the DEM is a promising technique for modelling the powder compaction process and analyzing the correlation between friction mechanism and force chains, but this application is rarely reported. According to our recent survey, two-dimensional (2D) and three-dimensional (3D) powder compaction have attracted much attention.[9,30–32] Although the mechanical behavior of powder is widely investigated by 3D simulation, the 2D simulation can also be used to study the densification of powders in a cross section and reveal the mechanical characteristics.[30,31] Sun and Ji[31] investigated the anisotropy of force networks by the 2D DEM model. They found that the 2D model can capture mechanical behavior in powder compaction accurately. Kruyt and Rothenburg[32] studied the isobaric experiments on granular materials by the 2D DEM model, and the study showed that the 2D simulation can accurately describe the anisotropic phenomena among particles. Besides, the visualization degree of force chains is higher indicated by 2D discrete element simulation. In present research, our goal is to ascertain the correlations between frictional effects and the force chain by the 2D discrete element method and their usefulness for improving the density and density homogeneity of green compacts. In this paper, we mainly study the physical properties of non-lubricated ferrous powder during powder compaction, and analyze the friction properties of powder compaction from the perspective of force chain dominated multi-scale mechanics, the said method is applicable to the physical phenomena exhibited during the compaction of ferrous powders, and then, the nonlinear physical responses between particles in the compaction stage of powder metallurgy are revealed. The dynamic friction characteristics of ferrous powders in powder compaction are analyzed from three scales: microscopic (between ferrous powders), microscopic (force chain formed by particles under specific physical conditions), and macroscopic (force chains formed by ferrous powders compaction).This study provides a theoretical basis for powder compaction forming technology through analyzing the condensed matter physical of ferrous particles. The main research contents are as follows:

(i) According to the actual working conditions, a discrete element model is established to conduct powder compaction experiments, and the Heckel equation is used to verify the powder compaction process.

(ii) Using the advantage of the DEM, the large principal stress criterion method is employed to extract the information about the force chain (such as the number and length of force chains, the proportion between high stress particles and force chain particles, and the distribution of force chain directions), a feature which is prepared for the subsequent quantification.

(iii) The correlation between the quantized information about force chain and the frictional behaviours (such as the motivation friction coefficient of the side wall and the motivation friction coefficient and slip ratio between particles) during powder compaction is analyzed.

1.1. DEM modeling

The DEM is a numerical method proposed by Cundall and Strack in 1979,[12] and differs from the description of granule matter in the theory of the finite element method.[33] In the DEM particle system, the force-displacement law is obtained.[34]

$$\boldsymbol{F}_{\mathrm{c}} = \boldsymbol{F}^{\mathrm{h}} + \boldsymbol{F}^{\mathrm{d}}, \tag{1}$$

where $\boldsymbol{F}^{\mathrm{h}}$ and $\boldsymbol{F}^{\mathrm{d}}$ are the nonlinear hertz force and dashpot force, respectively. Both forces are resolved into normal force and shear force as follows:[34]

$$\boldsymbol{F}^{\mathrm{h}} = -\boldsymbol{F}_{\mathrm{n}}^{\mathrm{h}}\hat{n}_{\mathrm{c}} + \boldsymbol{F}_{\mathrm{s}}^{\mathrm{h}}, \tag{2}$$

$$\boldsymbol{F}^{\mathrm{d}} = -\boldsymbol{F}_{\mathrm{n}}^{\mathrm{d}}\hat{n}_{\mathrm{c}} + \boldsymbol{F}_{\mathrm{s}}^{\mathrm{d}}, \tag{3}$$

where $\hat{n}_{\mathrm{c}}$ represents the direction normal to the contact plane, $\boldsymbol{F}_{\mathrm{n}}^{\mathrm{h}}$ and $\boldsymbol{F}_{\mathrm{s}}^{\mathrm{h}}$ denote the hertz normal force and hertz shear force, respectively, $\boldsymbol{F}_{\mathrm{n}}^{\mathrm{d}}$ and $\boldsymbol{F}_{\mathrm{s}}^{\mathrm{d}}$ indicate the dashpot normal force and dashpot shear force, respectively. The hertz normal force is given by

$$\boldsymbol{F}_{\mathrm{n}}^{\mathrm{h}} = -\frac{2\langle G\rangle\sqrt{2\bar{R}}}{3(1-\langle\nu\rangle)}|g_{\mathrm{c}}|^{3/2}, \tag{4}$$

where $\langle G\rangle$, $\bar{R}$, $\langle\nu\rangle$, and $|g_{\mathrm{c}}|$ are the equivalent elastic shear modulus, radius, Poisson's ratio, and contact gap, $(|g_{\mathrm{c}}| \le 0)$ respectively. The interparticle contact diagram is shown in Fig. 1, and the force between the particles or the force between the particles and the wall is calculated by the quantity of overlaps (gap) between the particles. The equivalent elastic shear modulus and Poisson's ratio are calculated as follows:

$$\langle G\rangle = \frac{(G_1+G_2)}{2}, \tag{5}$$

$$\langle\nu\rangle = \frac{(\nu_1+\nu_2)}{2}, \tag{6}$$

where G_1 and G_2 are the elastic shear moduli of two adjacent particles, ν_1 and ν_2 are the Poisson's ratios of two adjacent particles. The equivalent radius of contact can be expressed as

$$\frac{1}{\bar{R}} = \frac{1}{2}\left(\frac{1}{R_1}+\frac{1}{R_2}\right), \tag{7}$$

where R_1 and R_2 are the radii of two adjacent particles. The normal tangent stiffness is given by

$$k_{\mathrm{n}} = \left[\frac{\langle G\rangle\sqrt{2\bar{R}}}{(1-\langle\nu\rangle)}\right]\delta_{\mathrm{n}}^{1/2}, \tag{8}$$

where δ_{n} is the contact displacement increment of the normal direction. The Hertz shear force is given by

$$\boldsymbol{F}_{\mathrm{s}}^{\mathrm{h}} = k_{\mathrm{s}}\Delta\delta_{\mathrm{s}}, \tag{9}$$

where the $\Delta\delta_{\mathrm{s}}$ is relative shear-displacement increment, while the tangent shear stiffness is given by[34]

$$k_{\mathrm{s}} = \left[\frac{2(1-\nu)\langle G\rangle\sqrt{2\bar{R}}}{(2-\langle\nu\rangle)(1-\langle\nu\rangle)}\right]\left|\boldsymbol{F}_{\mathrm{n}}^{\mathrm{h}}\right|^{1/3}. \tag{10}$$

The dashpot shear force, $\boldsymbol{F}_{\mathrm{s}}^{\mathrm{d}}$, and the dashpot normal force, $\boldsymbol{F}_{\mathrm{n}}^{\mathrm{d}}$, can be calculated from

$$\boldsymbol{F}_{\mathrm{s}}^{\mathrm{d}} = \left(2\beta_{\mathrm{s}}\sqrt{m_{\mathrm{c}}k_{\mathrm{s}}}\right)\dot{\delta}_{\mathrm{s}}, \tag{11}$$

$$\boldsymbol{F}_{\mathrm{n}}^{\mathrm{d}} = \left(2\beta_{\mathrm{n}}\sqrt{m_{\mathrm{c}}k_{\mathrm{n}}}\right)\dot{\delta}_{\mathrm{n}}, \tag{12}$$

where β_{n} is the normal critical damping ratio, β_{s} is the shear critical damping ratio, m_{c} is the effective inertial mass, and $\dot{\delta}_{\mathrm{s}}$ and $\dot{\delta}_{\mathrm{n}}$ are the relative tangential velocity of particle and relative normal velocity of particle, respectively.

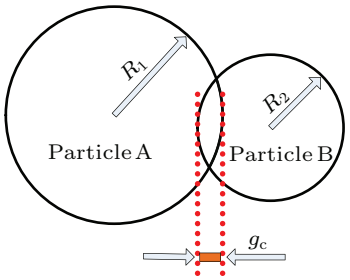


Fig. 1. Interparticle contact diagram.

To study the influence of friction on the mechanical behaviour of a granular system during powder compaction, a 2D particle model with a width of 0.02 m and a height of 0.02 m is established (Fig. 2). For the size of the simulation model, we conduct some work. With the height-to-width ratio increasing, the distribution of stress becomes more heterogeneous.[6] Reference [27] showed that the simulation model with a height-to-width ratio of 1:1 is suitable for studying the friction phenomenon of powder compaction. Moreover, the simulation model with a width of about 0.02 m has been widely studied,[6,27,29] so the simulation model with a width of 0.02 m and a height of 0.02 m is appropriate. The ferrous powder in this model has an initial relative density of 84% and then settled down under gravity (9.8 m/s^2). Particles are generated through grading.[35] In this work, the particles were generated by using the friendly interactive shell (FISH) command (number bin) in particle flow code (PFC). The FISH is a UNIX shell, the said programming language used to program particle flow. The PFC is a discrete element numerical analysis software based on granular matter theory. The particle sizes are divided into 11 segments, and each segment is uniformly distributed. The particle size distribution is shown in Fig. 3. The values of density, Poisson's ratio and elastic

modulus of particles are set according to the parameters of the ferrous powder.[29] The friction coefficient of ferrous powder is 0.25 based on Ref. [11]. To prevent particles from spilling out, the wall normal stiffness and the tangential stiffness are set to be 2×10^{12} N/m.[36] The detailed parameters are shown in Table 1. After generating the DEM model, the loading plate is compacted with a constant compaction velocity along the gravitational direction to achieve compaction until the axial strain reaches approximately 9%. At this axial strain, the corresponding pressure is approximately 640 MPa.[8,29]

Table 1. Model parameters.

Parameter name	Value	Parameter name	Value
Wall normal stiffness, k_n (N/m)	2×10^{12}	Particle size, r (μm)	150–200
Wall normal stiffness, k_s (N/m)	2×10^{12}	Particle mean diameter, $\langle D\rangle$ (μm)	350
Wall friction coefficient, μ_w	0.25	Particle friction coefficient, μ_p	0.25
Loading plate compaction velocity, V (m/s)	0.2	Particle density, ρ (kg/m^3)	7800
Normal damping coefficient, η_n (N·s/m)	0.7	Particle Poisson's ratio, ν	0.25
Tangential damping coefficient, η_s (N·s/m)	0.7	Particle elastic modulus, E (GPa)	209

To verify the reliability of the data, fitting Heckel equation is implemented. The compression behavior of the metal powder is widely analyzed by using the Heckel model.[37–39] Since the metals are densified by a similar compaction technology, and Heckel did his work by using the metal powders (powders of iron, steel, nickel, copper and tungsten[38]), so we choose Heckel equation to study the density–pressure relation. The equation is summarized by the compaction experiments on many metal powders:[38]

$$\ln\left(\frac{1}{1-D}\right)=KP+\ln\left(\frac{1}{1-D_0}\right), \tag{13}$$

where D and D_0 denote the relative density of the powder and the initial relative density of the powder, respectively, K is the proportional coefficient, and P is the upper die pressure stress.

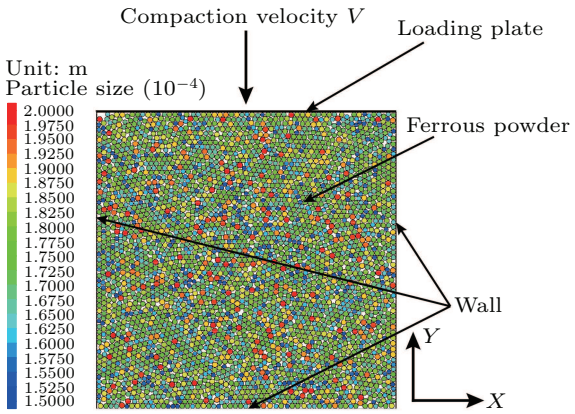


Fig. 2. DEM model.

The Heckel compaction equation fitting curve under powder compaction can be obtained by combining the data obtained from the powder compaction experiment as shown in Fig. 4, where e denotes the porosity of the ferrous powder, and the fitting curve is $\ln(1/e)=\left(1.075\times10^{-9}\right)P+1.864$. The linear correlation coefficient is R-square $=0.99496$, which indicates that the fitting curve has a high reliability because the value is close to 1. The experimental process of ferrous-base powder compaction fits the Heckel compaction equation. Note that this equation is inappropriate for low pressure compaction.[38]

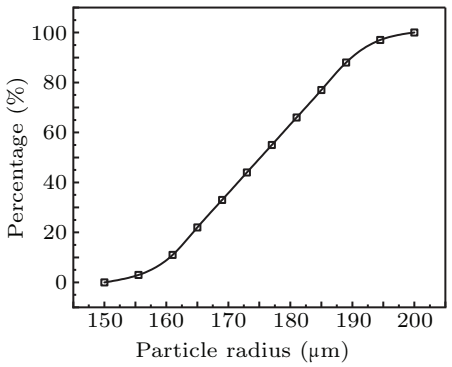


Fig. 3. Particle size distribution.

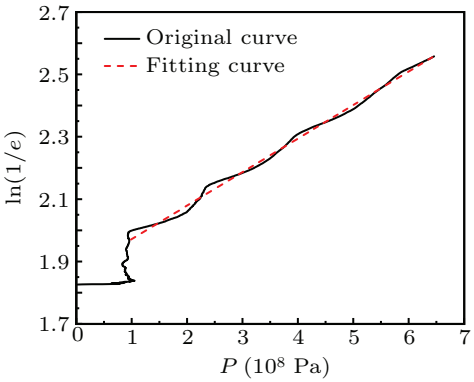


Fig. 4. Heckel equation during powder compaction.

2. Force chain retrieval algorithm

Several criteria currently exist for characterizing the force chain, such as the principal stress criterion and contact force criterion.[15,16,21,22,29] All these criteria define one force chain as a complex consisting of at least three particles. In this work, the force chain retrieval algorithm is obtained according to the recent literature.[13,16,21,22,25] To extract the information about

the force chain in the DEM, the rules are specified as follows.

(i) Rule of length The shortest force chains must have more than two particles.

(ii) Principle of high stress The major principal stress must be larger than the average major principal stress in the system. This criterion can be defined by Eqs. (14) and (15).

(iii) Angle rules for forming force chains The angle between the branch vector (the central line of the contact particles) and the direction of the major principal stress vector is less than 45°. The rule can be represented by Eqs. (16) and (17) as given below:

$$\sigma_1^j > \frac{1}{N}\sum_{i=1}^{N}\left|\sigma_1^i\right|, \tag{14}$$

$$\sigma_1^i = \frac{\sigma_{11}+\sigma_{33}}{2} + \sqrt{\left(\frac{\sigma_{11}-\sigma_{33}}{2}\right)^2 + (\sigma_{13})^2}, \tag{15}$$

where σ_1^{ij} is the major principle stress tensor, N is the total particle number, σ_{11} is the stress tensor in the x direction, σ_{33} is the stress tensor in the y direction, and σ_{13} is the stress tensor in the x to y direction.

$$\tan(2\theta) = \frac{2\sigma_{13}}{\sigma_{11}-\sigma_{33}}, \tag{16}$$

$$\cos\alpha < \frac{l\sigma_1^A}{|l|\left|\sigma_1^A\right|} \leq 1, \tag{17}$$

where θ is the direction of the major principle stress of the granule, α is the threshold set to be 45°. As shown in Fig. 5, granule A is the reference particle and granule B is an effective neighbour of A. The parameter l is a branch vector between the granules. σ_1^A is the major principal stress direction of particle A.

More detailed information about these rules can be found in the literature.[22] In addition, if two or more particles branch when the force chain grows, we choose the particle with the smallest angle (β). For example, particles B and C in Fig. 5 are high stress particles and are adjacent to particle A. However, when $\beta_1 > \beta_2$ then particle B is picked to be the force chain particle neighbor to particle A. The force chain is very sensitive to the change of external force, and when the external load changes, the force chain will evolve with it, such as through fracture and recombination.[21]

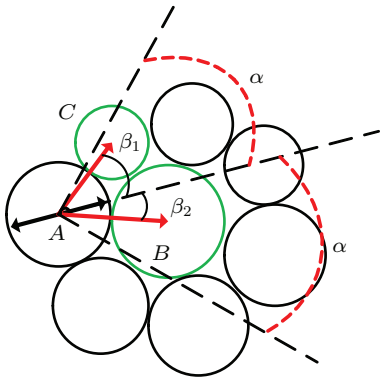


Fig. 5. Algorithm used to find force chains.

3. Result and discussion

3.1. Macroscopically characteristic analysis of force chain during powder compaction

Note that the properties of the force chain (such as its number, length and direction) are affected by the microscopic parameters of particles (including the friction characteristic between particles and the contact constitutive model).[22] To study the evolution of the force chain during powder compaction, we choose eight situations with axial strains, they being 0.5%, 1.5%, 2.0%, 2.5%, 3.0%, 6.0%, and 9.0%. The snapshots of force chains under the typical axial strain state are shown in Fig. 6.

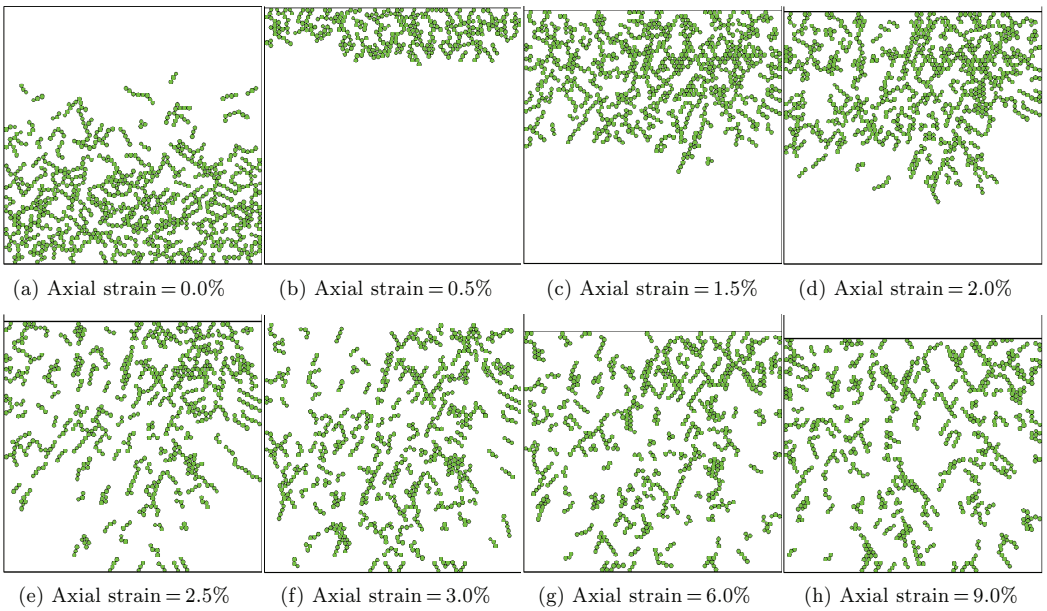


Fig. 6. Snapshots of force chain under typical axial strain state.

At the initial state and only under the action of gravity, the force chain is concentrated at the bottom of the particle system, and has strong randomness [Fig. 6(a)]. With the increase of the axial strain, the force chain begins to evolve from the top to the bottom of the particle system. This phenomenon occurs before the axial strain is approximately 2.5%, and then the force chain evolves throughout the particle system. With the increase of the axial strain, the force chain will gradually exhibit anisotropy [Figs. 6(e)–6(h)]. As the same time, further loading may cause the density of powder to increase and make the distribution of force chain more uniform.

To show the information about the force chain at each moment more intuitively, we quantify the length and number of the force chain. Figure 7 and Table 2 indicate the nexus between the length and number of force chains under different axial strains. However, no obvious change occurs in the distribution of the force chain length under different axial strains. Table 2 shows that longer chains is easier to form under low external loads, especially in the case of gravity alone (axial strain at 0.0%). As can be seen from Fig. 7 and Table 2, the number of force chains with force chain lengths 3 and 4 accounts for approximately 77% of the total number of force chains at the initial state. Meanwhile, the force chains with lengths greater than seven particles are relatively few, accounting for approximately 5%. With powder compaction, the force chain breaks easily and forms a shorter force chain. When the axial strain accounts for 0.5%, the longest length of the force chain is 12 particles; by contrast, when the axial strain occupies 9%, the longest length of the force chain is only 9 particles.

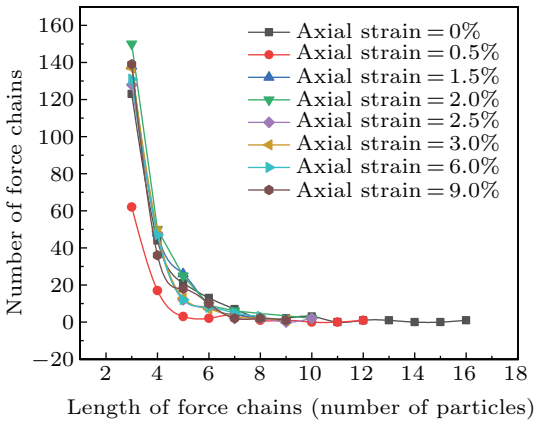


Fig. 7. Curves of force chain number versus length under different axial strains.

Table 2. Statistics of the number and length of force chains.

Number \ Length	3	4	5	6	7	8	9	10	11	12	13	14	15	16	Total
Axial strain=0.0%	123	44	21	13	7	2	2	3	0	1	1	/	/	1	218
Axial strain=0.5%	62	17	3	2	4	1	1	/	/	1	/	/	/	/	91
Axial strain=1.5%	138	48	26	9	4	2	1	/	/	/	/	/	/	/	228
Axial strain=2.0%	150	50	25	9	6	/	/	/	/	/	/	/	/	/	240
Axial strain=2.5%	128	48	12	8	2	2	/	2	/	/	/	/	/	/	202
Axial strain=3.0%	137	49	13	7	3	2	1	/	/	/	/	/	/	/	212
Axial strain=6.0%	131	47	12	8	5	3	/	/	/	/	/	/	/	/	206
Axial strain=9.0%	139	36	18	10	2	2	1	/	/	/	/	/	/	/	208

3.2. Correlation analysis of friction and force chain characteristics

The friction between the particles and the wall is the main reason that affects the uneven distribution of green density.[5,6] Thus, the friction characteristics of powder compaction must be analysed from two aspects.

The friction coefficient between particles and walls can be calculated by Coulomb's friction law.[40] The said law has been widely used to study the friction phenomena of granular matter.[9,27,29] The calculation method of Coulomb's friction law is specifically expressed in Eq. (18), where F_s and F_n are the shear and normal force acting on the side wall, the 'L' and 'R' denote the left side wall and right side wall, respectively. To study the average friction coefficients of all particles, we calculate the friction coefficients of all granules and divide the sum of friction coefficients by the total number of granules. The details are shown in Eq. (19).

$$\mu_{\text{wall}} = \frac{\left|F_s^{\text{L}}/F_n^{\text{L}}\right| + \left|F_s^{\text{R}}/F_n^{\text{R}}\right|}{2}, \tag{18}$$

$$\mu_{\text{particle}} = \frac{\sum_{i=1}^{N}\left|F_s^{\text{P}}/F_n^{\text{P}}\right|}{N}, \tag{19}$$

where F_s^{P} and F_n^{P} are the shear and normal forces received by all the particle. Levanov and Mater optimized the Coulomb friction equation and introduced the parameters such as the yield strength of the material when calculating the friction coefficient.[41] The friction constitutive equation has been used in Refs. [9,10]. The model can be represented by Eq. (20) in this study.

$$f = \frac{\sum_{i=1}^{N}\dfrac{\tau}{k\left(1-\exp\left(-1.25\left(q_n/\sigma_0\right)\right)\right)}}{N}, \tag{20}$$

where f is the friction factor, and τ and q_n represent the shear and normal stress, respectively, σ_0 is the initial yield stress of the ferrous powder, and has a value of 394 MPa. The parameter k is the yield stress in shear.

In our previous study, we confirmed a close relation between the friction coefficient of the side wall and the slip ratio of the granules adjacent to the side wall.[29] Meanwhile, the slip ratio and friction coefficient between granules are also worth further analyzing. Granule p is defined as the slip granule if the shear force between the other granule and granule p is near to the maximum static friction:

$$\begin{cases} \left|F_{\mathrm{s}}^{\mathrm{p}}\right| < 1.01\mu \left|F_{\mathrm{n}}^{\mathrm{p}}\right|, \\ \left|F_{\mathrm{s}}^{\mathrm{p}}\right| > 0.99\mu \left|F_{\mathrm{n}}^{\mathrm{p}}\right|. \end{cases} \tag{21}$$

After we identify the slip granules, we calculate the total number of slip granules and then divide it by the total number of granules to compute the slip ratio.

On the basis of the above theory, the evolution of the side wall friction coefficient with the axial strain during powder compaction is obtained [Fig. 8(a)]. The side wall friction has a similar variation tendency to experimental result in Ref. [11]. The friction coefficient increases almost linearly until the axial strain is nearly 1%. In our study, the friction coefficient of the side wall will eventually tend towards the steady state during powder compaction and is nearly 0.244. Figure 8(b) shows the average friction coefficients of different friction models for each particle during the powder compaction. In the initial phase, the friction coefficients of the two friction models both show a trend of linear growth, and then tend to move towards equilibrium. When the friction coefficient tends move towards equilibrium, the force chains exactly evolve from the top to the bottom (Fig. 6). The friction coefficient of the Levanov friction model finally tends to be 0.202, a value which is slightly lower than the friction coefficient of 0.25 which we set. However, the stable friction coefficient obtained from the Coulomb friction model is only 0.146 and remarkably differs from the value of friction coefficient that we set. Note that the Levanov friction model introduced more correction parameters than the Coulomb friction model, and previous studies proved that the Levanov friction model has a better improvement effect on the Coulomb friction model.[9,10] We find that the coefficient of the friction between particles is related to the following two aspects: on the one hand, the friction coefficient is related to the stress uniformity and this phenomenon can be represented by the force chain evolution process (see Fig. 6); on the other hand, the said coefficient is closely related to the slip ratio between particles [see Fig. 8(d)].

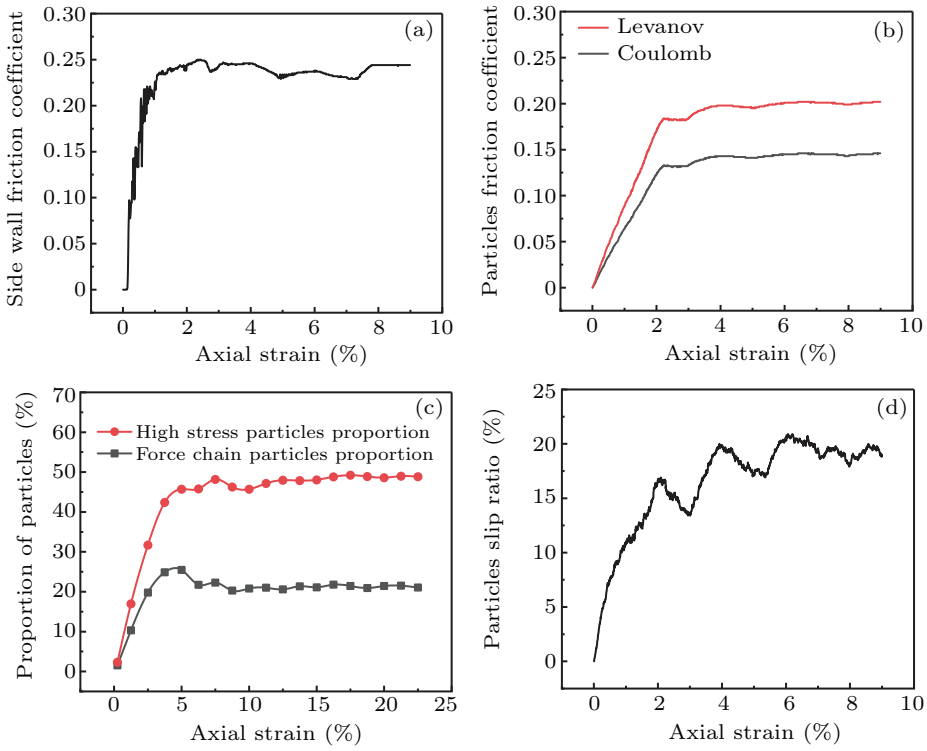


Fig. 8. Evolutions of (a) side wall friction coefficient, (b) mobilized particle friction coefficient, (c) proportion of high stress and force particles, and (d) slip ratio of particles with axial strain.

In Figs. 8(b) and 8(c), the evolution of the proportion of high stress particles and the evolution of force chain particles have the same trend as that of the friction coefficient. Remarkably, the proportion between the force chain particles and the high stress particles reaches the equilibrium ahead of the friction coefficient between particles arriving at the equilibrium. This phenomenon is caused mainly by a sudden decrease of the slip ratio between particles when the axial strain reaches 2%, thereby resulting in jamming[42,43] (see Fig. 6(d)), and the process continues until the axial strain is 2.5% [see Fig. 8(d)]. In this state, the high stress particles are mostly concentrated at the top of the model, and forming a force chain more easily

according to the judgment rule of the force chain angle. The jamming phenomenon will be investigated in our subsequent work.

In addition, the evolution of the friction coefficient between particles can also be explained by the previously analysed law of force chain evolution (see Fig. 6). The force chains grow from top to bottom during the initial stage of powder compaction. Between the axial strain of 2% and 2.5%, the force chain grows extensively to the lowest end of the particles, and the friction coefficient arrives at approximately equilibrium position. Therefore, the coefficient of the friction between particles is highly related to the uniformity of the stress between particles. As shown in Figs. 8(b) and 8(d), the friction coefficient and slip ratio between particles increase steadily before the axial strain of 2%. In an axial strain range from 2% to 3%, the slip decreases obviously, and the friction coefficient between particles also decreases. The friction coefficient between particles and the slip ratio first increase and then decrease in a range between 3% and 5% of axial strain, and then gradually stabilize.

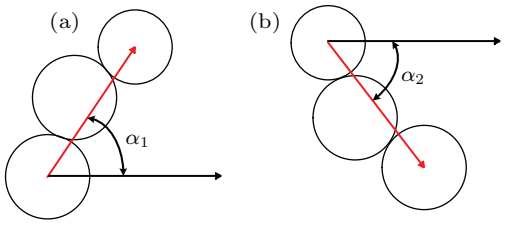


Fig. 9. (a) Positive angle and (b) negative angle of the force chain.

On the one hand, the friction between the side wall and the particles has a strong relation with the distribution of the side wall force chains, on the other hand, friction characteristic between all the granules are closely related to the evolution of force chains. Thus, the relation between the side wall and all interparticle friction should be investigated further. Reference [44] identifies a strong anisotropy in the direction of the principal stress of the particles near the side wall due to the friction between the side wall and the particles. Thus, we define the direction of the force chains as being similar but not equivalent to those in previous work.[22,25] The similarity is that the direction of the force chains is defined as the vector of the particles at the beginning and end of the force chain, but we propose a new angle distribution of the force chain. The angle of the force chain direction as shown in Fig. 9 (where we take a force chain of three particles for example) is between plus and minus 90° relative to the horizontal axis. The red arrows represent the direction of the force chains, and the angle can be computed from the tangent function. Meanwhile, the directivities of the force chains with different areas are studied quantitatively. We evenly divide the model into three parts to examine the anisotropy of the force chain direction.

Powder compaction can be divided into two stages: the particle rearrangement stage and the powder further compaction stage.[29] In this study, the axial strain before 2.5% should belong to the phase of particle rearrangement because the force chain has not fully evolved to the bottom of the die walls.

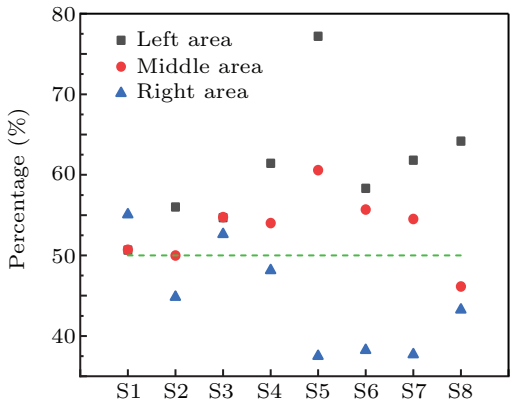


Fig. 10. Percentages of positive directions of force chains in different areas during powder compaction.

Figure 10 shows the percentages of the positive directions of force chains in different areas during various axial strains. Different states correspond to different axial strains. The S1–S8 states have an axial strain of 0.0%, 0.5%, 1.5%, 2.0%, 2.5%, 3.0%, 6.0%, and 9.0%, respectively. Given the friction in the further compaction stage of the powder (Fig. 10), the positive force chain in the middle area is distributed, arriving at approximately 50%, the positive force chain on the left side is distributed, reaching approximately 60% to 65%, and the positive force chain in the right area is distributed, accounting for about 40%. Thus, the ratio between positive and negative force chains in the left area and the right area are relatively higher. At the same time, it is noted that the sum of the proportion of force chains in the positive direction and the proportion of force chains in the negative direction is 100%. Therefore, the proportion of the force chains in the negative direction can be readily ascertained by examining the proportion of the chain of forces in the positive direction. All in all, the direction of the force chains in the middle area cannot be maintained in a constant positive or negative direction. The direction of the force chains in the middle area remains in a disordered state because the side wall friction has less effect on the force chain in the middle area. Nevertheless, the direction of the force chains occupying the left area remains positive after the particle rearrangement stage, and the direction of the force chains occupying the right area remains negative. It is certain that the side wall friction and the friction between particles would have an important effect on the direction of force chains growing in about one-third of the area near the side wall. The detailed probability distributions of the direction of the force chains are shown in Figs. 11–13.

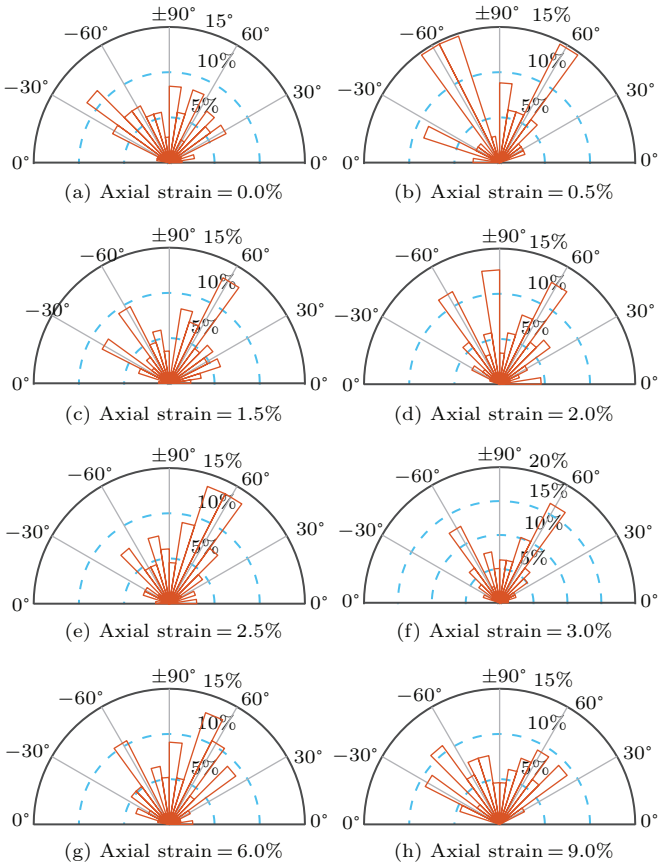


Fig. 11. Distributions of the force chain in the middle area for various axial strains.

As shown in Figs. 11–13, we divide the angles of the force chain in a range from -90° to $+90^\circ$ into 20 equal parts, calculate the percentage of the force chains in each angle interval, and draw a diagram of the probability distribution of the force chain in each direction. Figure 11 shows the probability distribution of the force chain direction in the middle area. The number of force chains in the positive direction and in the negative direction are almost equal. However, given the interaction between the lateral wall and the friction between the particles, we can confirm the anisotropy of the particle principal stress direction, and similar conclusions are reached in Ref. [44]. Meanwhile, the direction of the principal stress directly affects the evolution of the force chain, so the force chain close to the side wall will show strong directional changes. When the powder is compacted, the force chain near the left wall is dominant in the positive direction. (see Fig. 12). However, the direction of the force chain near the right wall is mostly in the negative direction (see Fig. 13). Further, the direction of the force chain during its evolution would converge to some angles. For example, the angle of the force chain close to the left tends to be approximately in a range from 30° to 70°, whilst the angle of the force chain close to the right tends to be approximately in a range from -30° to -70°. Nevertheless, the force chain in the middle area is disordered.

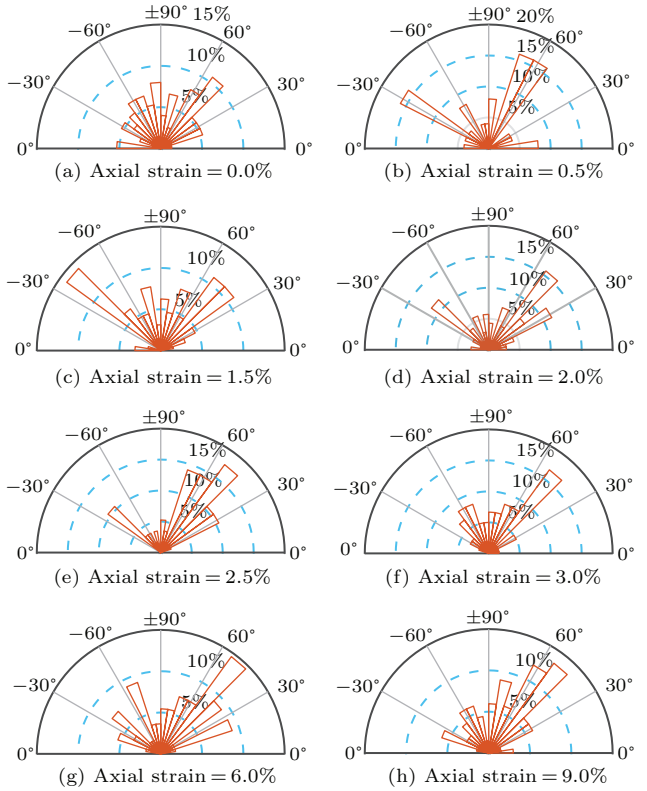


Fig. 12. Distributions of force chain in left area.

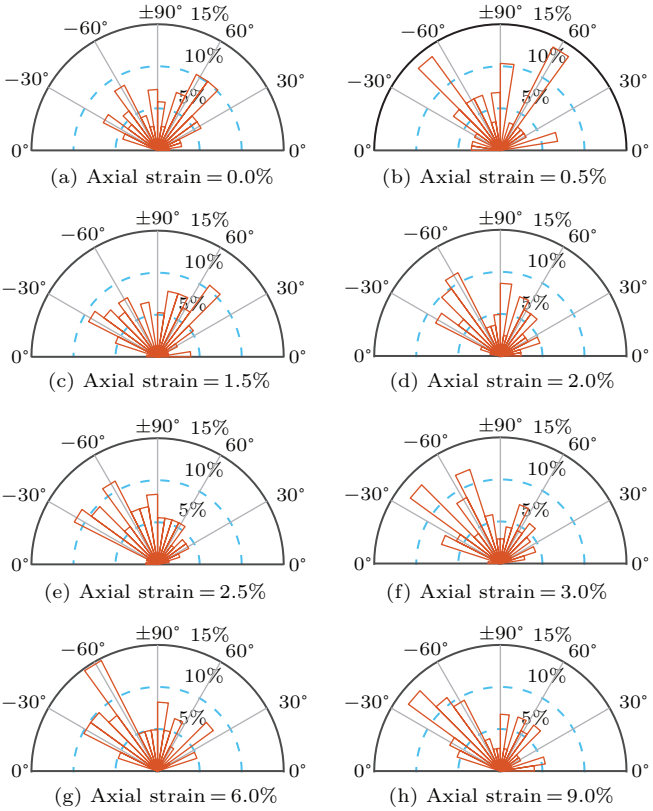


Fig. 13. Distributions of force chains in the right area for various axial strains.

According to Refs. [45,46], when powder is compressed or sheared, the anisotropy phenomenon exists in the normal and tangential forces of the particles. In this work, the direc-

tion of the major stress of the force chain is mixed with the directions of the tangential force and of the normal force of the particle. Therefore, the aggregation of the force chains in different directions may be related to the extent of anisotropy between the particle normal force and tangential force.

In Subsection 4.1, few force chains occur in the lower part of the force chains on both sides of the model during the macroscopic evolution of the force chains (see Fig. 6), the occurrence which is also related to the friction between the side wall and all particles. In other words, the friction will lead to lower stress near to the lower area of the side wall, which is similar to the research results in Ref. [44]. From the principle of densification, the friction will result in lower density near the side wall. Now, we can clearly establish that the frictional interaction between the side wall and all the particles influences the force chain. When the friction coefficient is close to zero, the green density may be higher. Reference [11] confirmed that under the lubrication action of zinc stearate, the reduction of the friction coefficient will enhance the densification effect, but the lubrication effect is limited; in addition, it is expected that more scholars will investigate this issue.

4. Conclusions

On the basis of the DEM, in this study the information about the force chain is extracted through the principal stress criterion method and the correlation between the force chains and the friction mechanism is investigated. The main research conclusions are as follows.

(i) With the increase of the axial strain, the force chain begins to evolve downward with the loading direction and fills the entire region when the axial strain is close to 2.5%. During loading, forming shorter force chains is easier. Under the action of gravity, the longest force chain reaches 16 particles, but when the axial strain reaches 9%, the length of the longest force chain is 9 particles.

(ii) Given an increase in the axial strain, the side wall friction and average particle friction coefficient begin to increase and eventually tend to be stable. The evolution of the slip ratio between particles and of the average particle friction coefficient have the same trend.

(iii) The average particle friction coefficient is related to the evolution of the force chain. When the force chain is filled with the entire particle system, the average particle friction coefficient reaches a stable state, but numerous jamming phenomena arise in the evolution of the force chain, a feature which will affect the evolution process of the force chain to a certain extent. We will further analyze this problem in the future research.

(iv) The principal stress direction of the particles is affected by the friction between the side wall and the particles. The direction of the force chain in the one-third of near side wall area is significantly affected by friction. As the axial strain increases, the angle of the force chain close to the left die wall tends to be approximately in a range from 30° to 70°, whilst the angle of the force chain close to the right die wall tends to be approximately in a range from −30° to −70°. This phenomenon will affect the densification process of powder compaction. Appropriate lubrication would be helpful in improving the green density.

Acknowledgements

Project supported by the Natural Science Foundation of Fujian Province, China (Grant No. 2020J01869), the Initial Scientific Research Fund in Fujian University of Technology, China (Grant No. GY-Z19123), and the Fujian Provincial Science and Technology Guiding Project, China (Grant No. 2017H0002).

References

[1] Khosravani M R and Nasiri S 2020 *J. Intell. Manuf.* **31** 847
[2] Chen C Y, Xie Y C, Yan X C, Yin S, Fukanuma H and Huang R Z 2019 *Additive Manufacturing* **27** 595
[3] Dong D Y, Huang X S, Li G Y and Cui J J 2020 *Mater. Chem. Phys.* **253** 123449
[4] Garner S, Strong J and Zavaliangos A 2018 *Powder Technol.* **330** 357
[5] Michrafy A, Dodds J A and Kadiri M S 2004 *Powder Technol.* **148** 53
[6] Wang W C, Qi H, Liu P A, Zhao Y B and Chang H 2018 *Metals* **8** 537
[7] Shoaib M, Kari L and Azhdar B 2011 *Powder Technol.* **217** 394
[8] Wang J Z, Qu X H, Yin H Q, Yi M J and Yuan X J 2009 *Powder Technol.* **192** 131
[9] Güner F, Cora Ö N and Sofuoğlu H 2018 *Tribol. Int.* **122** 125
[10] Güner F, Lu H S and Cora M N 2016 *Tribol. Int.* **96** 1
[11] Chen W C, Wang J H, Wang S P, Chen P Q and Cheng J G 2020 *Mater. Sci. Tech. Lond.* **36** 1057
[12] Cundall P A and Strack O D L 1979 *Géotechnique* **29** 47
[13] Zhang W, Liu K, Zhou J, Chen R X, Zhang N and Lian G F 2020 *Phys. Scripta* **95** 65704
[14] Zhang W, Zhou J, Zhang X J, Zhang Y and Liu K 2019 *Mod. Phys. Lett. B* **33** 1950113
[15] Sun Q C, Jin F, Liu J G and Zhang G H 2010 *Int. J. Mod. Phys. B* **24** 5743
[16] Peters J F, Muthuswamy M, Wibowo J and Tordesillas A 2005 *Phys. Rev. E* **72** 41307
[17] Bouchaud J P, Cates M E and Claudin P 1995 *J. Phys. I France* **5** 639
[18] Xiu T X, Wang W, Liu K, Wang Z Y and Wei D Z 2018 *Adv. Manuf.* **6** 355
[19] Fang Y G, Guo L F and Hou M X 2020 *Powder Technol.* **363** 621
[20] Mahabadi N and Jang J 2017 *Appl. Phys. Lett.* **110** 41907
[21] Tian J Q and Liu E L 2019 *Powder Technol.* **354** 906
[22] Fu L L, Zhou S H, Guo P J, Wang S and Luo Z 2019 *Granul. Matter* **21** 52
[23] Zhang L R, Nguyen N G H, Lambert S, Nicot F, Prunier F and Djeran M I 2017 *Eur. J. Environ. Civ. En.* **21** 874
[24] Tordesillas A, Froyland G and Walker D M 2014 *Phys. Rev. E* **89** 32205
[25] Liu J Y, Wautier A, Bonelli S, Nicot F and Darve F 2020 *Int. J. Solids Struct.* **193** 222
[26] Wang W, Liu Y, Zhu G Q and Liu K 2014 *Wear* **318** 114
[27] Meng F J and Liu K 2018 *J. Korean Phys. Soc.* **72** 1179
[28] Zheng H, Wang D, Chen D Z, Wang M M and Behringer R P 2018 *Phys. Rev. E* **98** 32904

[29] Zhang W, Zhang S, Tan J J, Du J L and Zhang N 2020 *J. Phys. Soc. Jpn.* **89** 124602
[30] Jiang C L, Wang A, Zhao F, Shang H L, Zhang M J, Liu F S and Liu Q J 2019 *Acta Phys. Sin.* **68** 228301 (in Chinese)
[31] Sun Q C and Ji S Y 2011 *Chin. Phys. Lett.* **28** 064501
[32] Kruyt N P and Rothenburg L 2019 *Int. J. Solids Struct.* **165** 14
[33] Clough R W and Tocher J L 1965 *Finite element stiffness matrices for analysis of plates in bending*", in *Proceedings of the First Conference on Matrix Methods in Structural Mechanics*, pp. 515–545
[34] Cundall P A 1988 *Computer Simulations of Dense Sphere Assemblies*, in *Studies in Applied Mechanics*, Satake M and Jenkins J T, Editors (Elsevier) pp. 113–123
[35] Jiang M J, Yin Z Y and Shen Z F 2016 *Granul. Matter* **18** 1
[36] Elata D and Berryman J G 1996 *Mech. Mater.* **24** 229
[37] Baumard J F, Coupelle P. 1994 *J. Mater. Sci. Lett.* **13** 93
[38] Heckel R W 1961 *Trans. Metall. Soc. AIME* **221** 671
[39] Denny, P J 2002 *Powder Technol.* **127** 162
[40] Staf H and Larsson P L 2020 *Powder Technol.* **363** 569
[41] Levanov A N and Mater J 1997 *Process. Tech.* **72** 314
[42] Bi D, Zhang J, Chakraborty B and Behringer R P 2011 *Nature.* **480** 355
[43] Dong Y X, Zhang G H, Sun Q C Zhao X D and Niu X N 2015 *Chin. Phys. Lett.* **32** 126201
[44] Zhang W, Zhou J, Zhang X J and Liu K 2019 *J. Korean Phys. Soc.* **74** 660
[45] Wang P and Yin Z Y 2020 *Ocean Eng.* **215** 107921
[46] Hu Z, Zhang Y D and Yang Z X 2020 *J. Geotech. Geoenviron.* **146** 4020024